

Development of a multiport test bench and systematic measurements of cable bundles for automotive EMC tests

M. Gonser¹, C. Keller¹, J. Hansen¹, and R. Weigel²

¹Corporate Sector Research and Advance Engineering, Robert Bosch GmbH, Stuttgart, Germany

²Institute for Electronics Engineering, University of Erlangen-Nürnberg, Germany

Abstract. In this paper the development of a cable bundle test bench is described and exemplary results of the systematic measurement of cable bundles for automotive EMC tests are presented. The test bench consists of particularly developed adapter boxes and switch matrices, which allow together with a network analyzer to perform a network analysis with up to 32 ports and up to 1 GHz. Calibration and deembedding procedures are described and validated. Cable bundles that are characteristic to automotive EMC tests are investigated with respect to the number of wires within the cable bundle, the class of the cable bundle and the type of wires.

2002), only few contain measurement data. Within most of these (Ciccolella and Canavero, 1995; Sun et al., 2007; Steinmetz, 2006) the reasonable approach is, to measure one resulting quantity (e.g. common mode current) and compare it to respective simulations. Influence of some parameters by measurement are investigated in Castanié (2002).

This work aims at a more extended investigation of cable bundle parameters and at founding a sound data base for the validation of a stochastic cable bundle model. While the model is presented in Gonser et al. (2010a,b) this paper describes the particularly developed test bench required for measuring and presents measurements of real cable bundles.

1 Introduction

In recent years, the rising complexity of automotive electronics along with shorter development periods challenges many design aspects of automotive products. One major issue is electromagnetic compatibility (EMC) and simulation of associated measurement setups even at early design stages become desirable.

Practical experience with nominally equal setups as well as round robin tests reveal considerable measurement uncertainty. Besides other sources for this uncertainty, the flexible wires within the cable bundle contribute largely to deviations in measurement results. A stochastic cable bundle model for respective simulations therefore becomes inevitable. In order to validate such stochastic models, statistical measurement data of cable bundles are needed.

While the literature shows a broad variety of stochastic cable bundle models (e.g., Ciccolella and Canavero, 1995; Salio et al., 1999; Sun et al., 2007; Steinmetz, 2006; Castanié,

2 Cable bundle test bench

2.1 Overview

Figure 1 shows an overview of the complete test bench. The *cable bundle*, which rests on styrofoam at height h above the table, is connected to *adapter boxes* at each end. Each of the adapter boxes is connected by *secondary measurement cables* to a *switch matrix*. Unused connectors of the adapter box are terminated with $50\ \Omega$ SMA terminations. Finally, each of the switch matrices is connected through the *primary measurement cables* to a *vector network analyzer* (NWA). The adapter boxes together with the actual cable bundle form the *device under test* (DUT) and the respective reference planes are located as indicated in Fig. 1. The setup is controlled by a PC, which is connected to the switch matrices via USB and to the NWA via GPIB (Fig. 3). Automated calibration, measurement and deembedding procedures are implemented in MATLAB. A measurement with all 32 ports and 1000 frequency points takes approximately 8 min.



Correspondence to: M. Gonser
(markus.gonser@de.bosch.com)

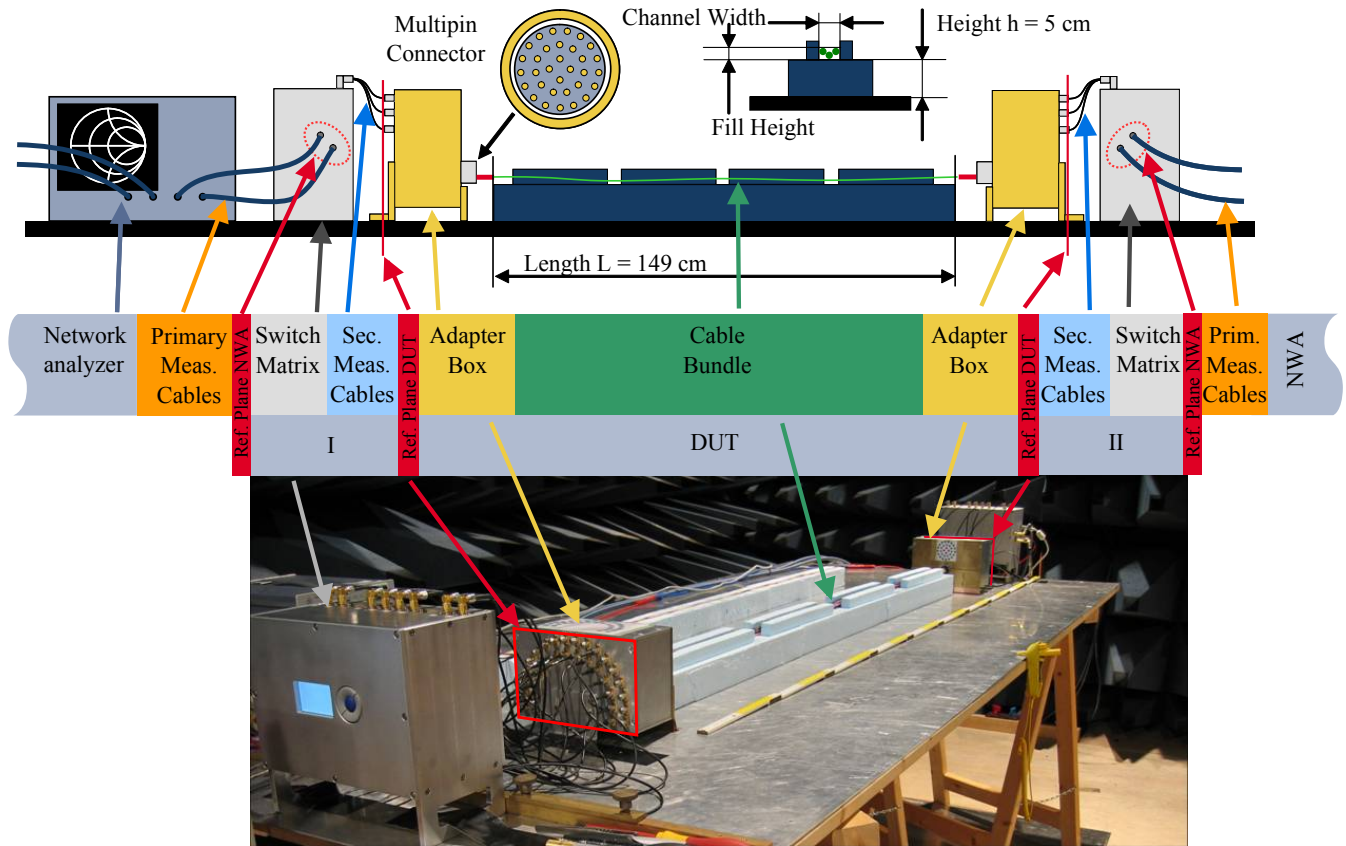


Fig. 1. Overview of the complete test bench.

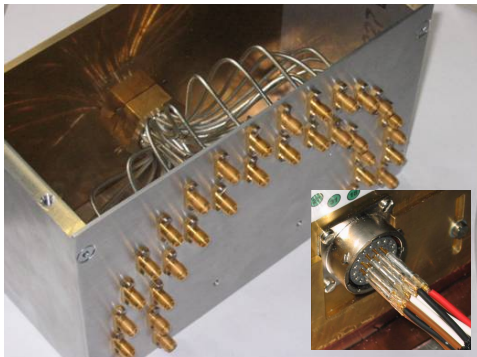


Fig. 2. Adapter box and multipin connector.

2.2 Adapter box

Figure 2 shows the inside of the adapter box and close-up view of the multipin connector. The use of the latter provides a quick and repeatable connection of the wires. Using coaxial semi rigid cables inside the box assures 50Ω line impedance up to the back of the multipin connector, and is favourable in order to perform network analysis. Each adapter box can accommodate up to 32 wires.

2.3 Switch matrix

As shown in Fig. 3 the switch matrix consists of three main printed circuit boards (PCB) in a housing made of alloy:

- *High Frequency PCB*: The four layer PCB is made of high frequency substrate. The two inner layers are ground layers and a total of 64 relays (2 per housing) are hosted on both outer layers of the PCB. The electromechanical high frequency relays are connected via grounded coplanar microstrip lines with a line impedance of $Z_W = 50 \Omega$ to each other in a topology, which allows the routing of each of the two NWA-sided ports arbitrarily to any of the 16 DUT-sided ports. All other DUT-sided ports are terminated with 50Ω .
- *Driver PCB*: The driver PCB serves two purposes: providing the relays with current when they are selected and shielding the high frequency part of the box from the digital part of the box.
- *Microcontroller PCB*: A microcontroller, USB to UART converter, LCD and control buttons are hosted on a third board, mounted on the back of the front panel.

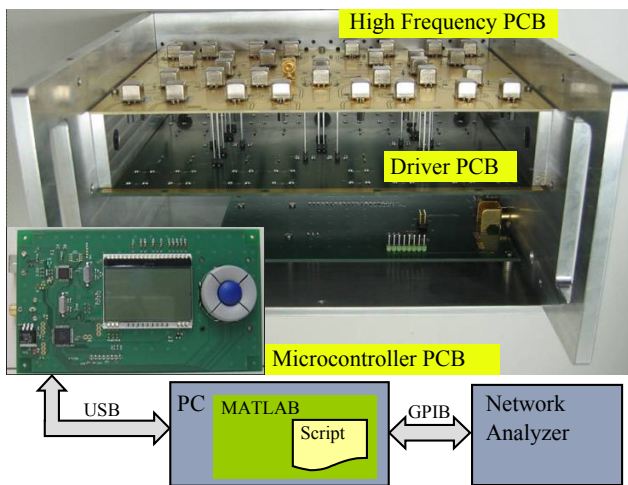


Fig. 3. Components and logical setup of the switch matrix

2.4 Multiport network analysis

2.4.1 Working principle

In order to measure cable bundles with many wires a system for network analysis with many ports is required. This can be achieved by a switching matrix, which automatically reroutes the ports available on the NWA to the different ports on the DUT. Two switch matrices were built. Each of the two switch matrices I and II has two ports on the side of the NWA, denoted A and B for switch matrix I and denoted C and D for switch matrix II. On the side of the DUT, each switch matrix has 16 ports, denoted 1 through 16.

While the network analyzer together with the switch matrices allow for many setups, only the case of using a four port NWA and both switch matrices is considered in this paper. Further, the total (even) number of used ports shall be split equally between both switch matrices. Without loss of generality, the secondary measurement cables are not mentioned separately, as they can be treated as part of their switch matrix. The primary measurement cables are accounted for by the calibration of the NWA itself.

Figure 4 shows a schematic of this setup. In order to measure the scattering parameter $\underline{S}^{\text{DUT}}(2n_w \times 2n_w)$ of the DUT, many measurements $\underline{S}_m^{\text{M}(4 \times 4)}[\text{A B C D}]$ with the NWA have to be performed. For the m -th measurement, ports A and B of switch matrix I are routed to ports i and j and ports C and D of switch matrix II are routed to the ports k and l respectively. This shall be expressed by the *path setting* $\mathbf{P}_m = [i \ j \ k \ l]$. Ports i , j , k , and l of the switch matrices are connected to ports $i' = i$, $j' = j$, $k' = k + n_w$, and $l' = l + n_w$ of the DUT. One possible set of path settings, which covers all ports of the DUT is:

$$\mathbf{P}_m \in \{[i \ j \ k \ l] \mid (1 \leq i \leq n_w) \wedge (i < j \leq n_w) \wedge (k = i) \wedge (l = j)\} \quad (1)$$

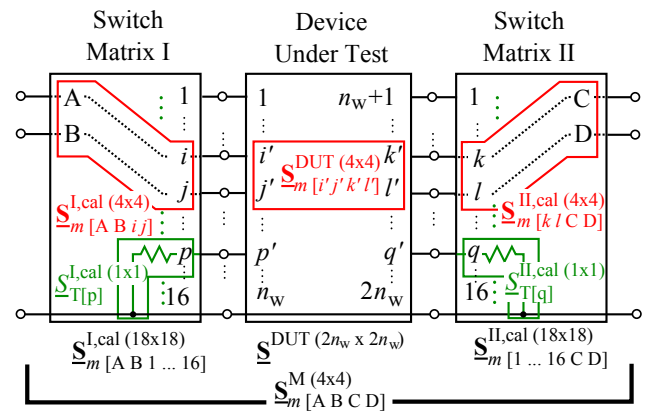


Fig. 4. Schematic of the setup.

Which results in a number of

$$N_M = \binom{n_w}{2} \quad (2)$$

total measurements, which have to be performed.

2.4.2 Calibration

Theoretically, for each of the N_M path settings \mathbf{P}_m the full 18 port scattering parameters $\underline{S}_m^{\text{I,cal}(18 \times 18)}[\text{A B 1} \dots \text{16}]$ and $\underline{S}_m^{\text{II,cal}(18 \times 18)}[\text{1} \dots \text{16 C D}]$ had to be measured, which would result in impractical amount of calibration data. However, the design of the switch matrix provides high isolation between all ports that are not involved in the current measurement, as well as high isolation of these ports to the ports involved in the current measurement. Therefore, only the subsets $\underline{S}_m^{\text{I,cal}(4 \times 4)}[\text{A B } i \ j]$ and $\underline{S}_m^{\text{II,cal}(4 \times 4)}[\text{k l C D}]$ are determined. Additionally, for all ports that are connected to the DUT, their non-ideal terminations $\underline{S}_m^{\text{I,cal}(1 \times 1)}[\text{T}[p}]$ and $\underline{S}_m^{\text{II,cal}(1 \times 1)}[\text{T}[q}]$ seen by the DUT, need to be determined.

2.4.3 Measurement

In order to perform the actual measurement, for every path setting \mathbf{P}_m of Eq. (1) a measurement $\underline{S}_m^{\text{M}(4 \times 4)}[\text{A B C D}]$ with the NWA is performed. The measurement is then transformed to transfer parameters $\underline{\mathbf{T}}_m^{\text{M}(4 \times 4)}[\text{A B C D}]$ as described in Appendix B. Similarly, the calibration data $\underline{S}_m^{\text{I,cal}(4 \times 4)}[\text{A B } i \ j]$ and $\underline{S}_m^{\text{II,cal}(4 \times 4)}[\text{k l C D}]$ are transformed to the respective transfer parameters. As switch matrices and DUT form a chain of network elements, the transfer parameters of the DUT are then:

$$\underline{\mathbf{T}}_m^{\text{DUT}(4 \times 4)}[\text{i' j' k' l'}] = \underline{\mathbf{T}}_m^{\text{I,cal}(4 \times 4)}[\text{A B } i \ j]^{-1} \underline{\mathbf{T}}_m^{\text{M}(4 \times 4)}[\text{A B C D}] \underline{\mathbf{T}}_m^{\text{II,cal}(4 \times 4)}[\text{k l C D}]^{-1} \quad (3)$$

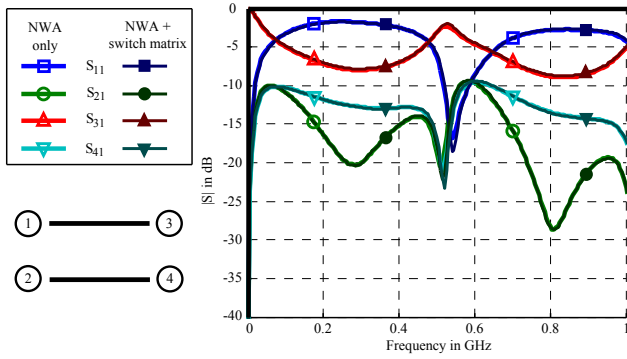


Fig. 5. Validation of the test bench.

These transfer parameters are under the premise, that all other ports of the DUT are terminated by ideal 50 Ω. In reality this is not the case and to account for the non-ideal termination at the DUT the method in Rautio (1983) is applied. It requires the calculation of the Gamma-R parameters (see Appendix C) of this measurement:

$$\underline{\mathbf{T}}_m^{\text{DUT}}(4 \times 4) \rightarrow \underline{\mathbf{S}}_m^{\text{DUT}}(4 \times 4) \quad (4)$$

$$\underline{\mathbf{S}}_m^{\text{DUT}}(4 \times 4) \xrightarrow{\Gamma_{[i \ j \ k \ l]} = \underline{\mathbf{S}}_T[i \ j \ k \ l]} \underline{\mathbf{R}}_m^{\text{DUT}}(4 \times 4) = \underline{\mathbf{R}}_m \quad (5)$$

These Gamma-R parameters $\underline{\mathbf{R}}_m$ are inserted in the matrix

$$\underline{\mathbf{R}}_{[1 \dots 2n_w]}^{\text{DUT}}(2n_w \times 2n_w) = \begin{matrix} & i' & j' & k' & l' \\ & \downarrow & \downarrow & \downarrow & \downarrow \\ i' \rightarrow & \left[\begin{array}{cccc} \underline{R}_{m11} & \dots & \underline{R}_{m12} & \dots & \underline{R}_{m13} & \dots & \underline{R}_{m14} & \dots \\ \vdots & \ddots & \vdots & \ddots & \vdots & \ddots & \vdots & \ddots \\ j' \rightarrow & \underline{R}_{m21} & \dots & \underline{R}_{m22} & \dots & \underline{R}_{m23} & \dots & \underline{R}_{m24} & \dots \\ \vdots & \ddots & \vdots & \ddots & \vdots & \ddots & \vdots & \ddots \\ k' \rightarrow & \underline{R}_{m31} & \dots & \underline{R}_{m32} & \dots & \underline{R}_{m33} & \dots & \underline{R}_{m34} & \dots \\ \vdots & \ddots & \vdots & \ddots & \vdots & \ddots & \vdots & \ddots \\ l' \rightarrow & \underline{R}_{m41} & \dots & \underline{R}_{m42} & \dots & \underline{R}_{m43} & \dots & \underline{R}_{m44} & \dots \\ \vdots & \ddots & \vdots & \ddots & \vdots & \ddots & \vdots & \ddots \end{array} \right] & \end{matrix} \quad (6)$$

Diagonal entries will be covered by more than one measurement, however all measurements for one diagonal entry provide the same data. Once all N_M measurements are pasted in $\underline{\mathbf{R}}^{\text{DUT}}$ it can be transformed back to the appropriate scattering parameter

$$\underline{\mathbf{R}}_{[1 \dots 2n_w]}^{\text{DUT}}(2n_w \times 2n_w) \xrightarrow{\Gamma = \underline{\mathbf{S}}_{\Gamma[1 \dots 2n_w]}^{(2n_w \times 2n_w)}} \underline{\mathbf{S}}_{[1 \dots 2n_w]}^{\text{DUT}}(2n_w \times 2n_w) \quad (7)$$

which is the final deembedded measurement

$$\underline{\mathbf{S}}_{[1 \dots 2n_w]}^{\text{DUT}}(2n_w \times 2n_w)$$

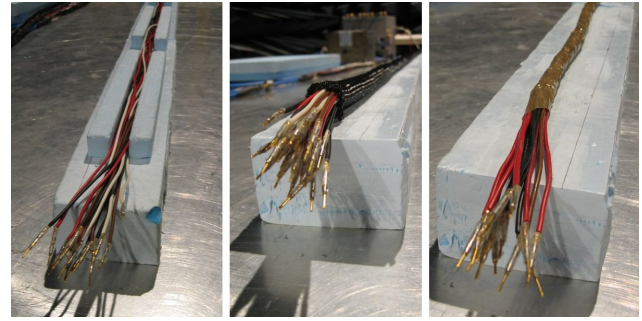


Fig. 6. Cable bundle classes (from left to right: channel of styrofoam, braided sleeve, taped).

2.5 Validation

The test bench is validated by a short two wire structure ($n_w = 2$), which is inserted into the adapter boxes. The resulting 4 ports were measured directly with the NWA, as well as with the two switch matrices in place. The comparison is shown in Fig. 5 and both measurements agree very well with each other, confirming the presented multiport measurement method up to 1 GHz.

3 Cable bundle measurements

3.1 Overview and analysis

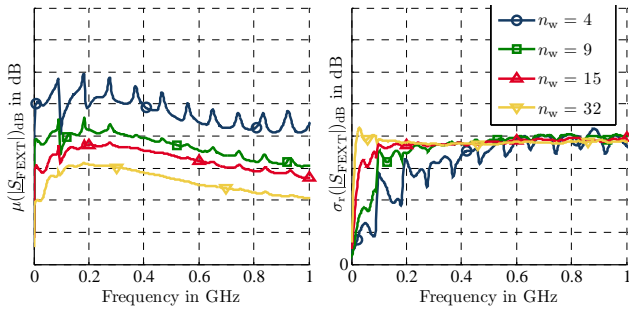
Table 1 shows an overview of the measured cable bundle configurations. The number of wires n_w , the size of the wire cross section A_w and the cable bundle class are varied. As shown in Fig. 6, classes of cable bundles are wires in a channel made of styrofoam, wires in a braided sleeve and wires wrapped by tape. While not all possible configurations are covered, parameters were chosen in such a way, that every parameter can be studied.

For every cable bundle configuration many specimen are generated and measured. In the case of styrofoam, the loose wires just have to be put newly in place. For the braided sleeve and the taped cable bundle, every time the cable bundle has to be first disassembled and then assembled again. It has been taken care that enough specimen were measured for a sound set of statistical data – i.e. the convergence of the statistical analyzed data are assured. Up to $N_C = 100$ specimen are necessary, wires with a higher number of wires requiring less measurements N_C .

Finally, the measured scattering parameters $\underline{\mathbf{S}}_i^{\text{DUT}}$ are categorized into reflection $\underline{S}_{j,\text{REFL}}$, transmission $\underline{S}_{j,\text{TRAN}}$, near end crosstalk $\underline{S}_{j,\text{NEXT}}$, and far end crosstalk $\underline{S}_{j,\text{FEXT}}$. Each of the groups is analyzed by calculating the statistical mean value

Table 1. Overview of the measured cable bundle configurations.

#	n_w	A_w	Class	N_C
1	4	0.25 mm ²	Styrofoam	100
2	4	0.50 mm ²	Styrofoam	100
3	4	1.00 mm ²	Styrofoam	100
4	9	1.00 mm ²	Styrofoam	60
5	15	0.25 mm ²	Styrofoam	30
6	15	0.50 mm ²	Styrofoam	50
7	15	1.00 mm ²	Styrofoam	60
8	32	1.00 mm ²	Styrofoam	60
9	15	1.00 mm ²	Braided sleeve	50
10	15	1.00 mm ²	Taped	50


Fig. 7. Comparison of measurement results for $A_w = 1 \text{ mm}^2$ of class styrofoam for the variation of n_w (left: 5 dB/div, right: 1 dB/div).

$$\mu(|S_{\text{cat}}|) = \frac{1}{N_{\text{cat}}} \sum_{j=1}^{N_{\text{cat}}} |S_{j,\text{cat}}| \quad (8)$$

and empirical standard deviation

$$\sigma(|S_{\text{cat}}|) = \frac{1}{(N_{\text{cat}} - 1)} \sum_{j=1}^{N_{\text{cat}}} (|S_{j,\text{cat}}| - \mu(|S_{\text{cat}}|))^2 \quad (9)$$

where

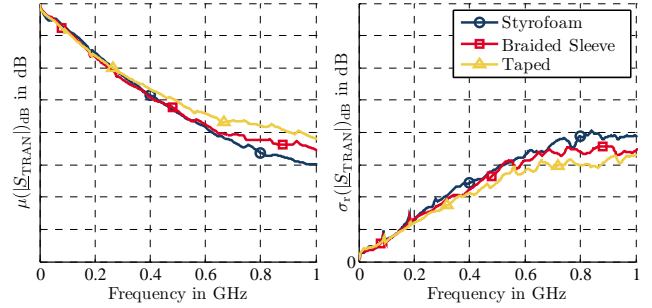
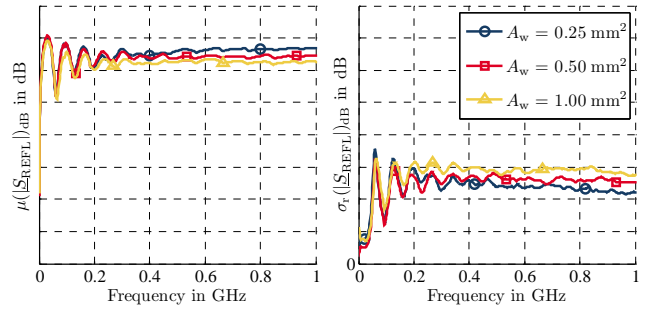
$$\text{cat} \in \{\text{REFL}; \text{TRAN}; \text{NEXT}; \text{FEXT}\}. \quad (10)$$

N_{cat} is the respective amount of measurements. For displaying purposes the logarithm is applied:

$$\mu(|S_{\text{cat}}|)_{\text{dB}} = 20 \log(\mu(|S_{\text{cat}}|)) \quad (11)$$

The empirical standard deviation $\sigma(|S_{\text{cat}}|)$ is normalized by the mean value $\mu(|S_{\text{cat}}|)$ before applying the logarithm, which results in the relative empirical standard deviation:

$$\sigma_r(|S_{\text{cat}}|)_{\text{dB}} = 20 \log\left(\frac{\sigma(|S_{\text{cat}}|)}{\mu(|S_{\text{cat}}|)} + 1\right) \quad (12)$$


Fig. 8. Comparison of measurement results for $A_w = 1 \text{ mm}^2$ and $n_w = 15$ and for the variation of the class (left: 5 dB/div, right: 1 dB/div).

Fig. 9. Comparison of measurement results for $n_w = 15$ of class styrofoam for the variation of A_w (left: 5 dB/div, right: 1 dB/div).

3.2 Results

In the following, exemplary results are shown and discussed. If not otherwise mentioned, similar behaviour is observed also for the other categories *cat*.

Figure 7 shows the parameter study with respect to the number of wires $n_w \in \{4; 9; 15; 32\}$ by the example of far end crosstalk FEXT. Increasing the number of wires n_w leads to a decrease in the mean value $\mu(|S_{\text{FEXT}}|)_{\text{dB}}$. The reason is, that the power of the source is coupled to an increasing number of adjacent wires $n_w - 1$. Further, resonances deviate more in frequency for the single specimen resulting in a mean value $\mu(|S_{\text{FEXT}}|)_{\text{dB}}$ with smaller resonance peaks. The relative standard deviation $\sigma_r(|S_{\text{FEXT}}|)_{\text{dB}}$ is approximately the same for all configurations for frequencies above 500 MHz. Cable bundle configurations with many wires reach this asymptotical value at lower frequencies than configurations with less wires.

Variation in the cable bundle class generally shows only small deviations. Figure 8 shows this for the mean value $\mu(|S_{\text{TRAN}}|)_{\text{dB}}$ and relative standard deviation $\sigma_r(|S_{\text{TRAN}}|)_{\text{dB}}$ for the category transmission TRAN. Examining the bundles, it can easily be seen that cable bundles of the class taped wires are much closer together than cable bundles of the class styrofoam. Braided sleeve is in between. As the same order

is shown in Fig. 8 it is concluded that this change is due to the cable bundle density. Further, experience with a stochastic cable bundle model (Gonser et al., 2010a,b) show the same behavior in simulations, when the parameter density ρ of the model is varied.

Similar behavior can be observed from variation of the size of the wire cross section A_w as shown in Fig. 9, which displays the mean value $\mu(|S_{REFL}|)_{dB}$ and relative standard deviation $\sigma_r(|S_{REFL}|)_{dB}$ for the category reflection REFL. By experience during actual measurement it is assumed that the small variation of mean value $\mu(|S_{REFL}|)_{dB}$ and relative standard deviation $\sigma_r(|S_{REFL}|)_{dB}$ is also caused by variations of the cable bundle density. Thicker wires usually result in a more densely packed channel of styrofoam, than thinner wire types.

4 Conclusions

A test bench for measuring cable bundles is presented. It consists of a network analyzer, two adapter boxes and two switch matrices, which were particularly developed for this task. The test bench allows to perform a fully automated network analysis with 32 ports up to 1 GHz. Control and deembedding are implemented in MATLAB. The mathematical background of the calibration and measurement tasks are presented and validated against direct measurement with the network analyzer.

The test bench is used to systematically measure cable bundles of different configurations. The size of the wire cross section A_w , number of wires n_w and cable bundle class are varied and measurements for many of the resulting cable bundle configurations are performed. For each configuration up to 100 specimen were measured and analyzed. The influence of the parameters n_w , A_w and class are presented. As expected, the number of wires n_w has the greatest influence on the scattering parameter. Remarkably, at higher frequencies the relative standard deviation $\sigma_r(|S_{cat}|)_{dB}$ is unaffected by a change of the number of wires n_w . The variation of the cable bundle class and the variation of the wire type A_w – both resulting in a change of cable bundle density – only show small effect on the scattering parameter.

The measurements presented are the basis for the validation of a stochastic cable bundle model as presented in Gonser et al. (2010a,b). The test bench will be used in future investigations of more complex cable bundles.

Appendix A

Scattering parameters

All networks in this paper have an even number of ports, which share the same ground node. Hence, a network with $2n$ ports has $(2n + 1)$ nodes as shown in Fig. A1, the ports being equally split between both sides. As stated in Kurokawa

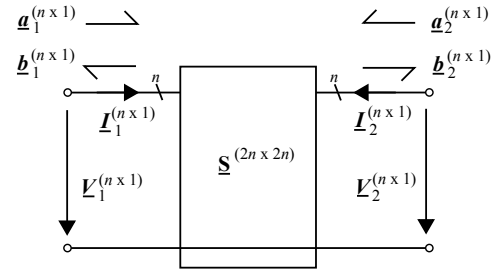


Fig. A1. Scattering parameter.

(1965), by using the nodal voltages \underline{V} and the currents \underline{I}

$$\underline{V}^{(2n \times 1)} = \begin{bmatrix} \underline{V}_1^{(n \times 1)} \\ \underline{V}_2^{(n \times 1)} \end{bmatrix} \quad \underline{I}^{(2n \times 1)} = \begin{bmatrix} \underline{I}_1^{(n \times 1)} \\ \underline{I}_2^{(n \times 1)} \end{bmatrix} \quad (\text{A1})$$

the following waves can be defined:

$$\underline{a}^{(2n \times 1)} = \underline{F}^{(2n \times 2n)} \left(\underline{V}^{(2n \times 1)} + \underline{G}^{(2n \times 2n)} \underline{I}^{(2n \times 1)} \right) \quad (\text{A2})$$

$$\underline{b}^{(2n \times 1)} = \underline{F}^{(2n \times 2n)} \left(\underline{V}^{(2n \times 1)} - \underline{G}^{+ (2n \times 2n)} \underline{I}^{(2n \times 1)} \right) \quad (\text{A3})$$

\underline{G} and \underline{F} are diagonal matrices where the i -th entry is the impedance of the i -th port \underline{Z}_i and $1/|\text{Re}(\underline{Z}_i)|$. The “+” denotes the complex conjugate transpose of the matrix. The scattering parameters \underline{S} are defined as:

$$\underline{b}^{(2n \times 1)} = \underline{S}^{(2n \times 2n)} \underline{a}^{(2n \times 1)} \quad (\text{A4})$$

Or divided by sides as in Fig. A1:

$$\begin{bmatrix} \underline{b}_1^{(n \times 1)} \\ \underline{b}_2^{(n \times 1)} \end{bmatrix} = \begin{bmatrix} \underline{S}_{11}^{(n \times n)} & \underline{S}_{12}^{(n \times n)} \\ \underline{S}_{21}^{(n \times n)} & \underline{S}_{22}^{(n \times n)} \end{bmatrix} \begin{bmatrix} \underline{a}_1^{(n \times 1)} \\ \underline{a}_2^{(n \times 1)} \end{bmatrix} \quad (\text{A5})$$

Appendix B

Transfer parameters

According to Klein (1976) the transfer parameters are

$$\begin{bmatrix} \underline{b}_1^{(n \times 1)} \\ \underline{a}_1^{(n \times 1)} \end{bmatrix} = \begin{bmatrix} \underline{T}_{11}^{(n \times n)} & \underline{T}_{12}^{(n \times n)} \\ \underline{T}_{21}^{(n \times n)} & \underline{T}_{22}^{(n \times n)} \end{bmatrix} \begin{bmatrix} \underline{a}_2^{(n \times 1)} \\ \underline{b}_2^{(n \times 1)} \end{bmatrix} \quad (\text{B1})$$

Transformation between \underline{S} and \underline{T} is

$$\underline{T} = \begin{bmatrix} \underline{S}_{12} - \underline{S}_{11} \underline{S}_{21}^{-1} \underline{S}_{22} & \underline{S}_{11} \underline{S}_{21}^{-1} \\ -\underline{S}_{21}^{-1} \underline{S}_{22} & \underline{S}_{21}^{-1} \end{bmatrix} \quad (\text{B2})$$

$$\underline{S} = \begin{bmatrix} \underline{T}_{12} \underline{T}_{22}^{-1} & \underline{T}_{11} - \underline{T}_{12} \underline{T}_{22}^{-1} \underline{T}_{21} \\ \underline{T}_{22}^{-1} & -\underline{T}_{22}^{-1} \underline{T}_{21} \end{bmatrix} \quad (\text{B3})$$

Appendix C

Gamma-R parameters

In order to correct non-ideal terminations, Gamma-R parameters $\underline{\mathbf{R}}$ are used as described in Rautio (1983). A new set of waves is defined as

$$\underline{\boldsymbol{\alpha}}^{(2n \times 1)} = \underline{\boldsymbol{a}}^{(2n \times 1)} - \underline{\boldsymbol{\Gamma}}^{(2n \times 2n)} \underline{\boldsymbol{b}}^{(2n \times 1)} \quad (\text{C1})$$

$$\underline{\boldsymbol{\beta}}^{(2n \times 1)} = \underline{\boldsymbol{\Gamma}}^{+(2n \times 2n)} \underline{\boldsymbol{a}}^{(2n \times 1)} + \underline{\boldsymbol{b}}^{(2n \times 1)} \quad (\text{C2})$$

$\underline{\boldsymbol{\Gamma}}$ is a diagonal matrix, where the i -th entry is the non-ideal termination $\underline{\Gamma}_i$ at the respective port. The important property is, that $\underline{\alpha}_i$ becomes zero when the i -th port is terminated by the non-ideal load $\underline{\Gamma}_i$. The definition of the Gamma-R parameters is

$$\underline{\boldsymbol{\beta}}^{(2n \times 1)} = \underline{\mathbf{R}}^{(2n \times 2n)} \underline{\boldsymbol{\alpha}}^{(2n \times 1)}. \quad (\text{C3})$$

Transformation from scattering parameters $\underline{\mathbf{S}}$ to Gamma-R parameters $\underline{\mathbf{R}}$ and vice versa is:

$$\underline{\mathbf{R}} = (\underline{\boldsymbol{\Gamma}}^+ + \underline{\mathbf{S}}) (\mathbf{1} - \underline{\boldsymbol{\Gamma}} \underline{\mathbf{S}})^{-1} \quad (\text{C4})$$

$$\underline{\mathbf{S}} = (\mathbf{1} + \underline{\mathbf{R}} \underline{\boldsymbol{\Gamma}})^{-1} (\underline{\mathbf{R}} - \underline{\boldsymbol{\Gamma}}^+) \quad (\text{C5})$$

References

- Castanié, C.: Modele de lignes de transmission non uniformes pour l'étude de couplages électromagnétiques sur des réseaux de câbles, Ph.D. thesis, L'Université Paul Sabatier, Paris, 2002.
- Ciccolella, A. and Canavero, F.: Stochastic Prediction of Wire Coupling Interference, in: IEEE Int. Symp. on Electrom. Compat., 51–56, 1995.
- Gonser, M., Keller, C., Hansen, J., and Weigel, R.: Advanced Simulations of Automotive EMC Measurement Setups Using Stochastic Cable Bundle Models, in: Asia Pacific EMC 2010, Beijing, China, 2010a.
- Gonser, M., Keller, C., Hansen, J., and Weigel, R.: Stochastisches Kabelbaummodell und dessen messtechnische Validierung für Kabelbäume in EMV-Komponentenmessverfahren der Automobilindustrie, in: EMV Düsseldorf, Düsseldorf, Germany, 2010b.
- Klein, W.: Mehrorttheorie, Akademie-Verlag Berlin, Berlin, Germany, 1976.
- Kurokawa, K.: Power Waves and the Scattering Matrix, IEEE Trans. on Microwave Theory and Technique, 13, 194–202, 1965.
- Rautio, J. C.: Techniques for Correcting Scattering Parameter Data of an Imperfectly Terminated Multiport When Measured with a Two-Port Network Analyzer, IEEE Trans. on Microwave Theory and Technique, 3, 407–412, 1983.
- Salio, S., Canavero, F., Lefebvre, J., and Tabbara, W.: Statistical Description Of Signal Propagation On Random Bundles Of Wires, in: 13th Int. Zurich Symp. on EMC, 499–504, 1999.
- Steinmetz, T.: Ungleichförmige und zufällig geführte Mehrfachleitungen in komplexen, technischen Systemen, Ph.D. thesis, Otto-von-Guericke-Universität Magdeburg, Magdeburg, 2006.
- Sun, S., Liu, G., Drewniak, J., and Pommerenke, D.: Hand-Assembled Cable Bundle Modeling for Crosstalk and Common-Mode Radiation Prediction, IEEE Trans. on Electromagn. Compat., 49, 708–718, 2007.